

Detecting macromolecular differences of the CSF in low disability multiple sclerosis using quantitative MT MRI at 3T

Richard D Lawless*  Colin D McKnight*  Kristin P O'Grady , Anna JE Combes ,
Baxter P Rogers, Atlee A Witt , Mereze Visagie, Delaney C Houston, Logan E Prock,
Francesca R Bagnato and Seth A Smith

Multiple Sclerosis Journal—
Experimental, Translational
and Clinical

October–December 2023,
1–10

DOI: 10.1177/
20552173231211396

© The Author(s), 2023.
Article reuse guidelines:
sagepub.com/journals-
permissions

Abstract

Background: Imaging investigation of cerebrospinal fluid (CSF) in multiple sclerosis (MS) is understudied. Development of noninvasive methods to detect pathological CSF changes would have a profound effect on MS diagnosis and would offer insight into MS pathophysiology and mechanisms of neurological impairment.

Objective: We propose magnetization transfer (MT) MRI as a tool to detect macromolecular changes in spinal CSF.

Methods: MT and quantitative MT (qMT) data were acquired in the cervical region in 27 people with relapsing-remitting multiple sclerosis (pwRRMS) and 38 age and sex-matched healthy controls (HCs). MT ratio (MTR), the B_1 , B_0 , and R_1 corrected qMT-derived pool size ratio (PSR) were quantified in the spinal cord and CSF of each group.

Results: Both CSF MTR and CSF qMT-derived PSR were significantly increased in pwRRMS compared to HC ($p=0.027$ and $p=0.020$, respectively). CSF PSR of pwRRMS was correlated to Expanded Disability Status Scale Scores ($p=0.045$, $R=0.352$).

Conclusion: Our findings demonstrate increased CSF macromolecular content in pwRRMS and link CSF macromolecular content with clinical impairment. This highlights the potential role of CSF in processing products of demyelination.

Keywords: Multiple sclerosis, cerebrospinal fluid, magnetic resonance imaging, spinal cord, magnetization transfer ratio

Date received: 11 April 2023; accepted 16 October 2023

Introduction

Multiple sclerosis (MS) is a chronic autoimmune disease of the central nervous system (CNS) and is the most prevalent neurological condition in young adults, with an estimated 1,000,000 cases in the United States and 2.5 million worldwide.¹ MS is characterized by inflammation, demyelination, and variable degrees of axonal degeneration. MRI is the primary diagnostic tool as it can identify brain and spinal cord lesions² over time. Conventional MRI, e.g., T1-weighted (T_1 -w) and T2-weighted (T_2 -w) images are sensitive to inflammatory lesions and tissue atrophy, but often poorly mirror clinical decline

and cannot assess the underlying pathophysiology of MS.³

Recent studies have highlighted the potential role of cerebrospinal fluid (CSF)-mediated metabolism of neurologic waste products.^{4,5} Tailored imaging focused on the CSF of MS patients offers potential insight into disease processes, however, MRI assessment of CSF in MS is unexplored. Conventional MRI of CSF has been limited to flow dynamics and volumetric measurements. T_1 -w and T_2 -w images of the CSF are overwhelmed by the water signal and are not sensitive to small changes in CSF composition.

*These authors contributed equally to the production of this manuscript.

Correspondence to:
Colin D McKnight,
Department of Radiology and
Radiological Sciences,
Vanderbilt University Medical
Center, 1211 Medical Center
Drive, Nashville, TN,
37232 USA.
colin.d.mcknight@vumc.org

Richard D Lawless,
Vanderbilt University Institute
of Imaging Science,



Vanderbilt University Medical Center, Nashville, TN, USA
Department of Biomedical Engineering, Vanderbilt University, Nashville, TN, USA

Colin D McKnight,
Department of Radiology and Radiological Sciences, Vanderbilt University Medical Center, Nashville, TN, USA

Kristin P O’Grady,
Vanderbilt University Institute of Imaging Science, Vanderbilt University Medical Center, Nashville, TN, USA
Department of Radiology and Radiological Sciences, Vanderbilt University Medical Center, Nashville, TN, USA
Department of Biomedical Engineering, Vanderbilt University, Nashville, TN, USA

Anna JE Combes,
Vanderbilt University Institute of Imaging Science, Vanderbilt University Medical Center, Nashville, TN, USA

Baxter P Rogers,
Vanderbilt University Institute of Imaging Science, Vanderbilt University Medical Center, Nashville, TN, USA
Department of Radiology and Radiological Sciences, Vanderbilt University Medical Center, Nashville, TN, USA

Atlee A Witt,
Mereze Visagie,
Delaney C Houston,
Logan E Prock,
Vanderbilt University Institute of Imaging Science, Vanderbilt University Medical Center, Nashville, TN, USA

Francesca R Bagnato,
Division of Neuroimmunology, Department of Neurology, Vanderbilt University Medical Center, Nashville, TN, USA
Department of Neurology, VA Hospital, TN Valley Healthcare System, Nashville, TN, USA

Seth A Smith,
Vanderbilt University Institute of Imaging Science, Vanderbilt University Medical Center, Nashville, TN, USA
Department of Radiology and Radiological Sciences, Vanderbilt University Medical Center, Nashville, TN, USA
Department of Biomedical Engineering, Vanderbilt University, Nashville, TN, USA

In white (WM) and gray matter (GM), demyelination is a hallmark of MS pathology, and previous studies have shown that magnetization transfer (MT) imaging is an indirect surrogate for demyelination in the CNS.^{6–8}

The MT ratio (MTR) is a clinically relevant method for characterizing the MT effect and has been shown to correlate with myelin density within WM,^{6,7,9} however, it is only semi-quantitative and depends on MRI scan parameters as well as water content which can confound accurate assessment of myelin change.^{10–12} Advanced, quantitative MT (qMT) is a model-based approach sensitive to myelin content. It removes dependencies on nonphysiological parameters and the influence of inflammation.^{7,13}

qMT utilizes T_1 , B_1 , and B_0 maps to fit MT-weighted signals as a function of offset frequency (z-spectra) to a 2-(or more) pool biophysical model and provides maps of physiological values such as the pool size ratio (PSR), which has been shown to be related to myelin content.^{14,15} MT-weighted MRI as well as qMT-derived PSR show MS abnormalities in superficial cord structures proximal to CSF in relapsing-remitting and progressive forms of the disease.¹⁶ MTR and qMT have generically been utilized in WM and GM of the brain and spinal cord to relate to myelination; however, these metrics have been often ignored in large water components such as the CSF because normal, healthy CSF does not generate MT contrast. Here, we hypothesize that if myelin products of demyelination aggregate in sufficient concentration within the CSF, an increased MT effect could be noted. If present, elevated MTR and PSR values within the CSF of MS patients could reflect important evidence of CSF-mediated clearance of products of demyelination in MS, though additional work would be needed to conclusively determine that these signal changes are not derived from alternative CSF content such as pro-inflammatory proteins. The goal of this study is to provide evidence of an increased MT effect in the CSF of MS patients and to assess the relationship between the abnormal MT in the CSF to MT changes within WM. We chose the

spinal cord and surrounding CSF because of the proximity of the spinal cord WM to the large pool of surrounding CSF.

Methods

Study cohort

The local Institutional Review Board approved this study and all participants provided signed informed consent prior to examination. Thirty-eight age and sex-matched healthy controls (HCs) participated (22 female/16 male, 22–40 years of age, average age 30.6 years), with seven returning for repeatability assessment. Twenty-seven people with relapsing-remitting multiple sclerosis (pwRRMS) meeting the revised McDonald’s Criteria (2) were consecutively recruited (17 female/10 male, 20–42 years of age, average age 34.9 years). All patients exhibited low disability (Expanded Disability Status Scale [EDSS] score range 0–2.5, median EDSS = 0).¹⁷

MRI protocol

Imaging was performed using a 3.0-T, Philips Elition X scanner (Philips Healthcare, Best, The Netherlands) with a quadrature body coil for excitation and a 16-channel neurovascular coil for reception. For each subject, we acquired a multi-echo fast-field echo (mFFE) as our anatomical reference and registration/segmentation target (details in Supplementary Data).¹⁸ qMT data were obtained as listed in Table 1. The qMT protocol used a 3D MT-prepared spoiled gradient echo sequence.¹³ The MT pre-pulse is a 20-ms single-lobed sinc-Gauss pulse, applied at a single power ($B_{1,MT} = 820^\circ$) and offset frequency ($\Delta\omega = 2.5$ kHz) for “single-point” qMT analysis^{14,19–21} and calculation of the MTR. The field-of-view (FOV) spanned the C2 to C5 vertebrae over 14 slices. Other parameters can be found in Table 1.

Image processing and analysis

All data analyses were performed in Matlab 2019b (Mathworks, Natick, MA). All MT-weighted images were cropped and diffeomorphically registered to

Table 1. Imaging parameters.

Scan	Resolution (mm3)	TR/TE (ms)	α	Scan time (m:s)
mFFE	0.65 × 0.65 × 5	TR/TE ₁ /ΔTE: 700/7.2/8.8	28°	5:30
qMT	1 × 1 × 5	TR/TE: 50/2.3	6°	7:00
B ₁	2 × 2 × 5	TR ₁ /TR ₂ /TE: 30/130/2.8	60°	1:12
B ₀	2 × 2 × 5	TR/TE ₁ /TE ₂ : 40/4.6/6.9	60°	0:45
MFA	1.5 × 1.5 × 5	TR/TE: 20/4.6	5, 15, 20, 25, 30°	1:30
				Total time: 15:57

the mFFE using the Advanced Normalization Toolbox.²² Similarly, B_0 , B_1 , and R_1 maps were coregistered to the first offset of the MT-weighted acquisition and transformed to the mFFE space. Observed relaxation rate ($R_{1,obs}$) maps were calculated by fitting multiflip angle (MFA) T1-weighted imaging data to the SPGR signal equation in the steady state²³ voxel by voxel. $R_{1,obs}$ is the calculated R_1 from the MFA measurement that has been B_1 corrected. Conventional qMT fitting requires the assumption of a specific saturation-lineshape, typically super-lorentzian in CNS tissue. However, no studies have confirmed the correct line-shape assumption for CSF, or even in healthy or damaged tissues. Because of the lack of knowledge about the line shape, and the unconventional approach of estimating the MT effect in the CSF, we chose to utilize the single-point qMT model. The single-point fitting approach utilizes the 2-pool MT model to apply T1, B_1 , and B_0 corrections to the MT-weighted signal at one offset frequency (e.g., the MTR) to generate an estimate of the PSR.²¹ Therefore, the offset frequency and RF amplitude were corrected on a voxel-by-voxel basis using the B_0 and B_1 maps, and the PSR was derived voxel-by-voxel utilizing the additional input of R_1 .

MTR and single-point qMT

Contrary to a qMT fit to the entire MT-weighted z-spectra obtained with multiple saturation parameters (full-fit model), for the single-point model, the exchange rate (k_{mf}), macromolecular T_2 ($T_{2,m}$), and free-pool T_2 ($T_{2,f}$) can be fixed, as they exhibit relatively constant values across tissue types,^{3,4} however they have only been studied in healthy WM and GM. The details for parameter estimation for the single-point qMT model in the spinal cord are shown in Smith et al.¹⁴ The remaining free parameter in the model, PSR, is then estimated using a single normalized MT-weighted scan at offset frequency and saturation power (MTR), which is corrected by B_1 , B_0 , and R_1 . In this work, values for fixed assumptions were selected to be those derived from WM and GM, and deviations from the assumptions could increase (or decrease) the observed PSR leading to a bias. While we recognize that a bias may exist by incorrectly assumed values for fixed parameters, since the same assumptions are utilized in both HC and pwRRMS, comparisons between cohorts can be evaluated. Lastly, the single-point fit, while it provides an estimate of the PSR, is, in fact, an MTR measurement that has been corrected for T1, B_1 , and B_0 , and a model is employed solely to apply these corrections. As such, the qMT acquisition was

also used to calculate standard MTR maps (without B_1 , B_0 , and T1 correction) using the equation:

$$MTR = \frac{M_0 - M_{sat}}{M_0} \quad (1)$$

where M_{sat} is the saturated, MT-weighted signal and M_0 is the reference signal without MT-saturation. For M_{sat} , we chose offset frequency ($\Delta\omega$) = 2.5 kHz, and $\Delta\omega = 100$ kHz offset was used for normalization, M_0 . Recall M_{sat} was coregistered to M_0 to minimize misregistration artifacts

WM, GM and CSF were automatically segmented from the mFFE using Spinal Cord Toolbox v3.2.7 (NeuroPoly, Montreal, Canada)²⁴ and applied to all other image types that were co-registered to the mFFE. Anatomical images in axial and sagittal planes, anatomy labels, and tissue segmentation are shown in Figure 1 for an HC subject. Note that the CSF was eroded around the contact with the cord to minimize partial volume effects with the spinal cord WM. CSF was selected as the area outside the spinal cord and within the spinal canal for the same C2–C5 FOV as seen in blue in Figure 1.

Statistical analysis

Statistical comparisons were performed on the mean values within each tissue type (WM, GM, and CSF). Box plots were created for both cohorts, comparing values of MTR, PSR, and $R_{1,obs}$ in each tissue type. A nonparametric Wilcoxon rank sum test was performed to determine any group differences in the mean PSR, MTR, and $R_{1,obs}$ values for each tissue type. The correlation of CSF PSR and WM PSR with EDSS score was assessed using Spearman Rank correlations. The correlation of SC PSR and WM PSR with CSF PSR was also assessed. Reproducibility was assessed using a Bland Altman test for both PSR and MTR in all tissue types over repeat visits in healthy volunteers. Reported are the normalized Bland-Altman difference (D_{BA}), 95% confidence interval, and the limits of agreement. A significance threshold of $\alpha = 0.05$ was used for all statistical analyses.

Results

Cohort differences

Anatomical mFFE, MTR, PSR, $R_{1,obs}$, B_1 , and B_0 maps for a representative HC and pwRRMS are displayed in Figure 2. MTR and PSR are decreased in the WM and GM of pwRRMS (blue and green) when compared to the HC (yellow and red). As expected, all MT indices are lower in CSF relative

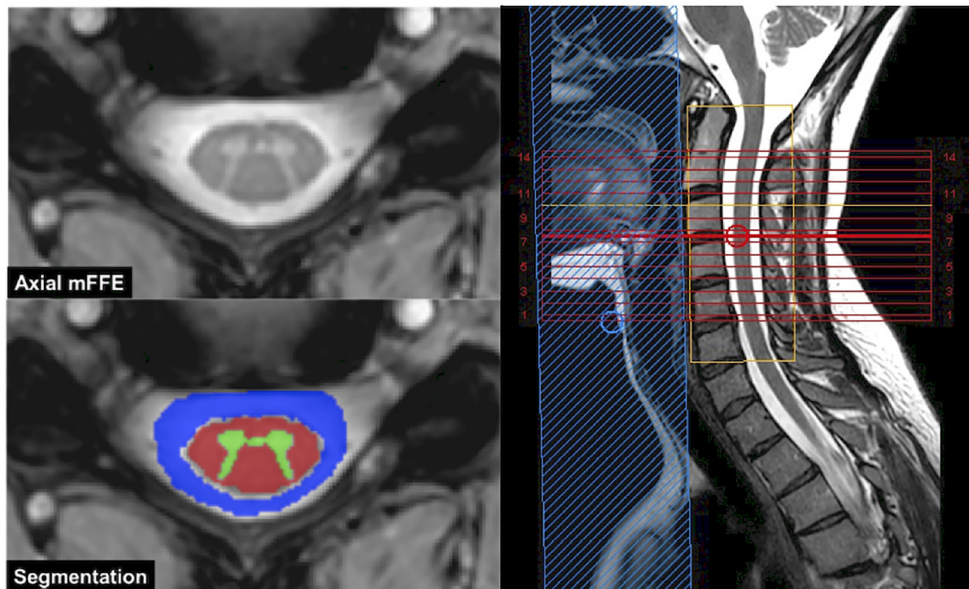


Figure 1. Axial anatomical image (left top) and segmentation (bottom left). Also shown is the sagittal T2 (right) with FOV (yellow box).
FOV: field of view.

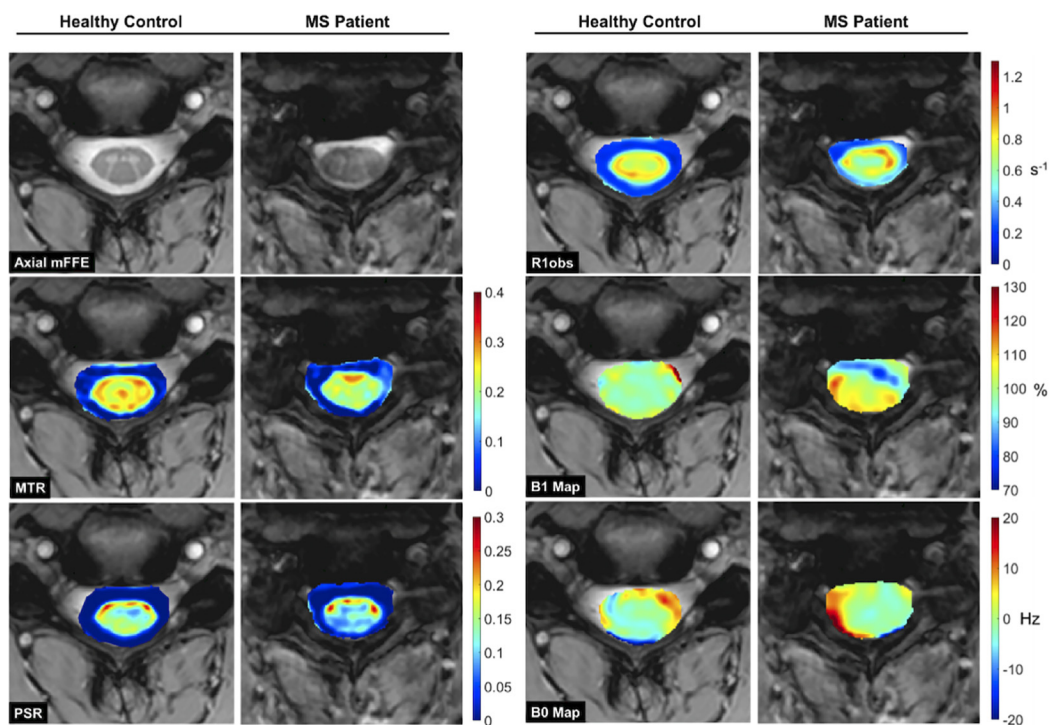


Figure 2. Anatomical data (a), MTR (b), PSR (c), $R_{1,obs}$ (d), B_1 map (e), and B_0 map (f) for representative healthy control (left column) and MS patient (right column). Observe the decrease in the MTR and PSR within the spinal cord of the MS patient when compared to the control, accompanied by increases in the surrounding CSF.
MTR: magnetization transfer ratio; PSR: pool size ratio; MS: multiple sclerosis; CSF: cerebrospinal fluid.

to spinal cord tissue. In pwRRMS, however, CSF MTR and PSR values are higher than in HC. The MTR map in one MS patient shows a mottled

appearance in the left lateral CSF, while PSR shows hyperintensity in the dorsal CSF. No notable differences are observed for $R_{1,obs}$ in either the GM, WM

Table 2. Mean tissue values.

	Patients			Healthy controls		
	MTR	PSR	R1OBS (S-1)	MTR	PSR	R1OBS (S-1)
CSF	$0.039 \pm 0.029^*$	$0.0032 \pm 0.0032^*$	0.33 ± 0.16	0.033 ± 0.024	0.0022 ± 0.0027	0.32 ± 0.12
WM	0.21 ± 0.033	$0.14 \pm 0.047^*$	0.78 ± 0.17	0.21 ± 0.031	0.16 ± 0.054	0.84 ± 0.15
GM	0.19 ± 0.035	$0.12 \pm 0.040^*$	0.76 ± 0.12	0.19 ± 0.023	0.13 ± 0.036	0.80 ± 0.10
L	0.18 ± 0.035	$0.11 \pm 0.040^*$	0.67 ± 0.12			

* $p > 0.05$.
MTR: magnetization transfer ratio; PSR: pool size ratio; CSF: cerebrospinal fluid; WM: white matter; GM: gray matter.

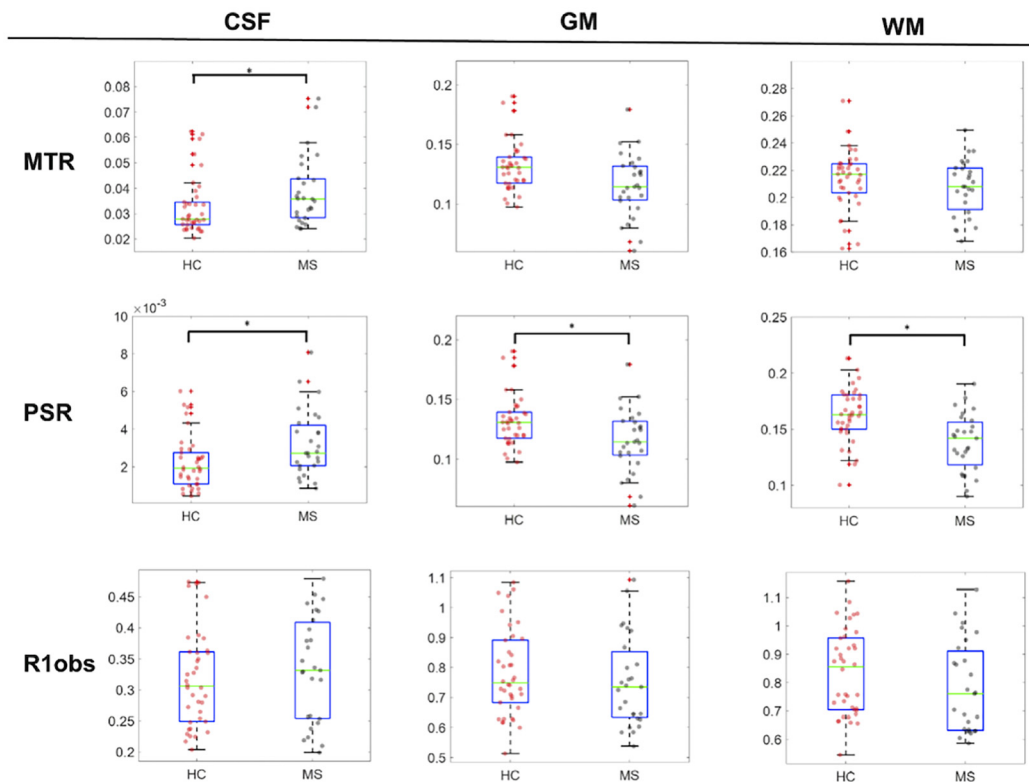


Figure 3. Cross cohort box plot comparison for MTR, PSR, and R1obs in each tissue type (CSF, WM, GM). Only CSF values exhibited significant differences in MTR ($p = 0.027$) and all tissue types were significantly different in PSR (pCSF = 0.020, pWM < 0.001, pGM = 0.023). In both MT measurements, values in patients are higher in the CSF and lower within the cord when compared to healthy controls. No differences were found in the R1obs values. (*: $p = 0.05$).

MTR: magnetization transfer ratio; PSR: pool size ratio; CSF: cerebrospinal fluid; WM: white matter; GM: gray matter.

or CSF. $R_{1,obs}$, B_1 , and B_0 maps are shown for completeness. Note, the differences in the B_0 and B_1 maps between these two individuals highlighting the need for B_1 , B_0 , and R_1 correction.

The mean and standard deviation for MTR, PSR, and $R_{1,obs}$ for each tissue type (CSF, WM, GM, Lesion) are shown in Table 2.

Figure 3 compares the mean values for each subject within the CSF, GM, and WM for the HC and pwRRMS groups. The MTR in the CSF was significantly higher in pwRRMS ($p = 0.027$) and trended lower in the GM and WM, though not statistically significant ($p = 0.255$, $p = 0.278$, respectively). PSR is significantly different in all tissue types, pwRRMS PSR is higher in CSF ($p = 0.020$) and lower in the

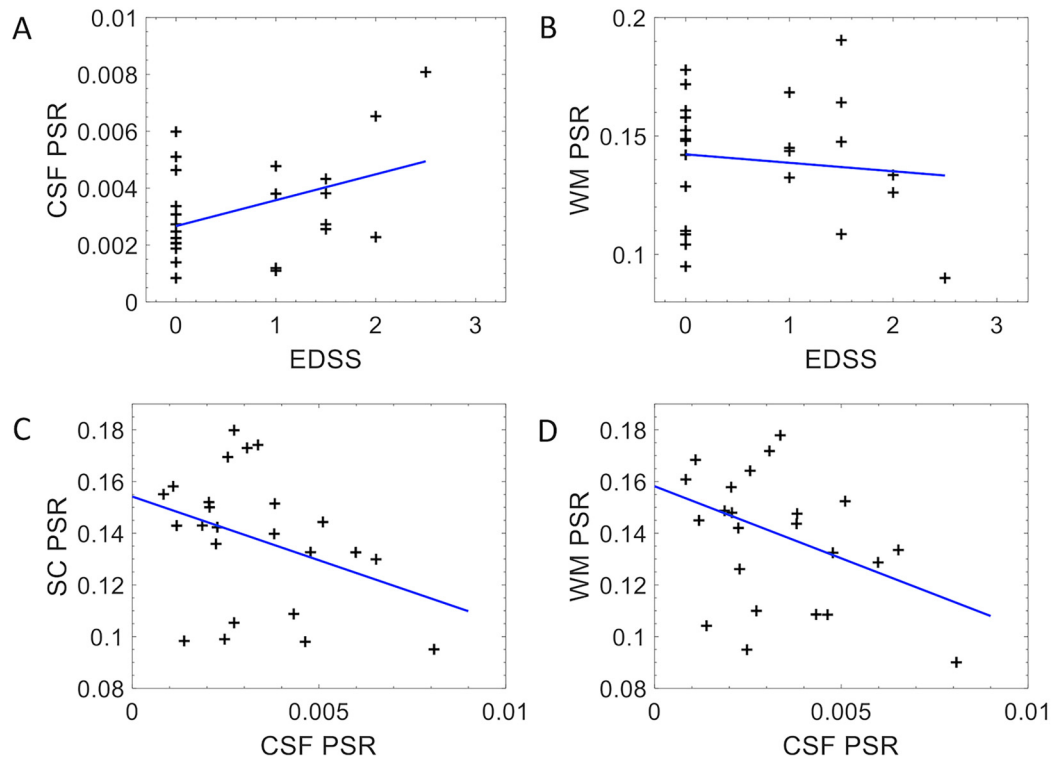


Figure 4. Correlation plots comparing CSF PSR in MS patients to expanded disability status scale (EDSS) score (A) ($p = 0.045$, $\rho = 0.352$) and WM PSR to EDSS (B) ($p = 0.866$, $\rho = -0.036$). Correlation plots comparing SC PSR to CSF PSR (C) ($p = 0.063$, $\rho = -0.371$) and WM PSR to CSF PSR (D) ($p = 0.095$, $\rho = -0.347$). PSR: pool size ratio; MS: multiple sclerosis; CSF: cerebrospinal fluid; WM: white matter.

GM ($p = 0.010$) and WM ($p < 0.001$). $R_{1,obs}$ are similar in the CSF of pwRRMS and lower in the GM and WM, but no significant differences were detected.

Associations among tissue types and clinical disability

Associations between CSF PSR and EDSS (A), WM PSR and EDSS (B), SC PSR and CSF PSR (C), and WM PSR and CSF PSR (D) as shown in Figure 4. In pwRRMS, CSF PSR is significantly correlated with EDSS ($p = 0.045$, $R = 0.352$) (4A), while WM PSR and EDSS were not correlated ($p = 0.866$, $R = -0.036$) (4B). CSF PSR exhibits a trending negative correlation with SC PSR ($p = 0.063$, $R = -0.371$) (4C), and a trending negative correlation with WM PSR ($p = 0.095$, $R = -0.347$) (4D).

Reproducibility

Reproducibility was assessed using Bland-Altman, interclass correlation coefficients (ICC) and mean coefficients of covariances for CSF and WM for both PSR and MTR as shown in Figure 5. For Bland-Altman analysis, the dotted red lines indicate the 95th percentile

confidence interval (± 1.96 SD), and in each imaging method and tissue type, overlaps 0, indicating no bias in the reproducibility estimate. Note, however, that the PSR measures are slightly more clustered around the mean difference. Regarding ICC, both measures, MTR and PSR in the CSF show strong reproducibility with $ICC = 0.74$ and 0.80 , respectively. When considering the WM, the ICC is slightly lower for the PSR and, due to the clustering of data, low for the MTR. Regarding the coefficients of variation, WM MTR and PSR are lowest ($< 10\%$) while the variation for CSF is higher. This is not unexpected as the MTR and PSR were designed to exploit contrast from WM and some optimizations need to be explored to improve both the model and sensitivity for CSF characterization. In all, reproducibility is in the moderate to strong range for both MTR and PSR for both tissue types.

Discussion

CSF imaging and MT indices

We demonstrated that MT (qMT-derived PSR and MTR) is abnormal in the CSF in pwRRMS compared to HC. In pwRRMS, we identified a negative correlation between

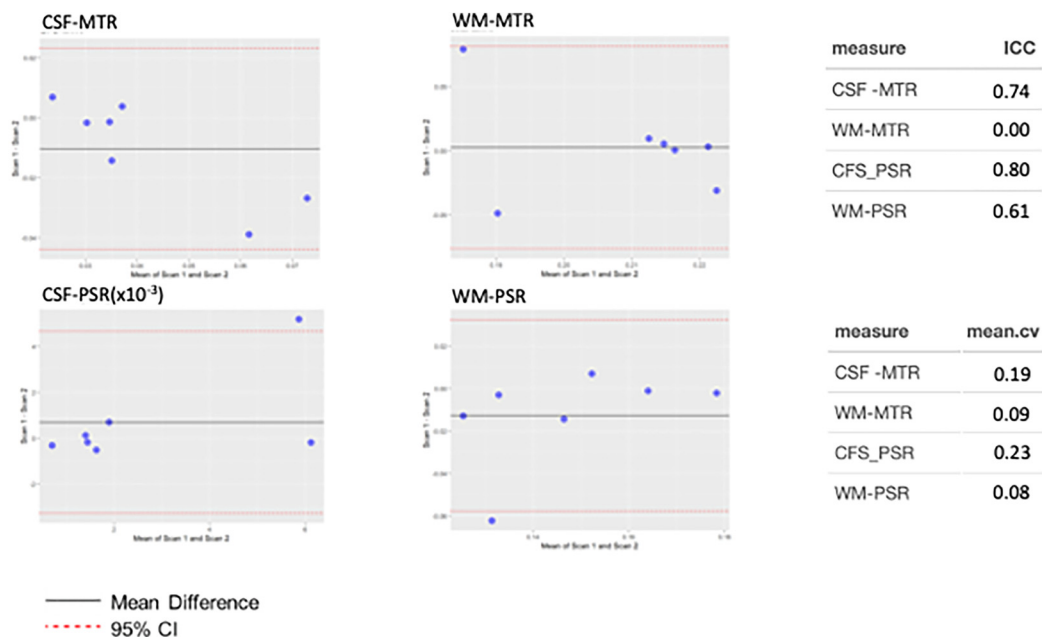


Figure 5. Evaluation of reproducibility for CSF MTR, WM MTR, CSF PSR, and WM PSR in healthy control subjects. Plots demonstrate Bland–Altman characterization of reproducibility, where red-dotted lines indicate 95% confidence interval of mean difference, black solid line shows the mean difference. In each plot, the 95th percentile overlaps 0, indicating no observable bias. CSF MTR and PSR show strong agreement as shown by ICC, with the latter showing slightly greater reproducibility compared to the former, however, the mean coefficient of variation for the former is lower than the latter. For WM, the ICC for MTR is clustered and does not show a strong correlation with follow-up, however, the coefficient of variation for WM MTR is low, as is WM PSR. It is expected that the variation in WM is lower as both the MTR and PSR are designed to be sensitive to white matter changes, more so than tailored for CSF evaluation. MTR: magnetization transfer ratio; PSR: pool size ratio; CSF: cerebrospinal fluid; WM: white matter.

WM PSR and CSF PSR, as well as a positive correlation between CSF PSR and clinical disability (EDSS). Finally, we demonstrated that both the PSR and MTR techniques are repeatable for both CSF and WM.

Despite the increasing evidence of CSF-mediated neurologic waste clearance, imaging of CSF has been limited to flow dynamics and volumetric measurements. This is primarily because of the limited information that can be provided by standard T_1 -w and T_2 -w images, and, until recently, no MRI methodology could provide evidence of CSF abnormalities in disease populations. MT imaging has a long history of providing indices sensitive to demyelination, however, has not been studied in the CSF due to the general, expected lack of macromolecular aggregates that would give rise to MT signals. However, we recognized that the CSF MT was different in HCs and patients with MS prompting a further evaluation into using MT as a probe for CSF abnormalities relating to MS *in vivo*.

Even though MTR is sensitive to non-physiological parameters,^{10,11} we included it in this evaluation

because it is the most commonly used method for evaluating MT changes in clinical practice, does not require fitting, or advanced modeling and yet has been shown to correlate with myelin concentration.⁷ qMT corrects for these nonphysiological dependencies and potential sources of error through application of R_1 , B_0 , and B_1 corrections using a model and can provide indices that are more physiologically linked such as PSR, which is also strongly associated with myelin density throughout the CNS.^{14,15,20} Our MT measurements within the SC are consistent with previous studies of demyelinating disorders^{14,15,20}: detecting decreased PSR and MTR in MS patients compared to HCs. Similarly, measures in the CSF indicate increased MT effect in the CSF of MS patients compared to controls, which, to our knowledge, is the first report of such a finding.

CSF-mediated CNS waste clearance and correlation to disability

Recent research pertaining to the glymphatic system indicates that the CSF serves as a critical mediator of CNS parenchymal waste products which traverse the subarachnoid CSF en route to clearance from the CNS. Our preliminary findings demonstrate

abnormal MT indices in the subarachnoid CSF pool of MS patients, which could reflect macromolecular waste product accumulation in the setting of MS. Other explanations for this finding include increased cellular content and increased proinflammatory proteins such as cytokines, chemokines and immunoglobulins. The increased CSF PSR of MS patients and the apparent negative correlation between PSR in the WM versus the CSF (although this did not reach statistical significance) raises the possibility of parenchymal to CSF demyelination product clearance that merits further investigation. CSF PSR also shows a correlation to EDSS, highlighting a potential biomarker of disease. Identifying imaging correlations to clinical measures of disability has long been an issue in radiological studies of MS.²⁵ Previous investigation has demonstrated substantially different cellular and protein content in ventricular CSF as compared to lumbar CSF in MS patients.²⁶ Future studies should measure the MT indices within the various CSF compartments to further characterize the etiology and significance of the elevated cervical CSF MT signal seen in MS patients in this study.

Study limitations and conclusions

While this study is preliminary and opens the door for further studies, we report some limitations to the current study. For qMT, we utilized an MT pulse sequence with saturation (saturation power, duration, and offset frequency) and readout (excitation flip angle, sequence TR) parameters optimized for SC GM and WM.²¹ However, we recognize that these pulse sequence parameters could be improved for CSF-specific imaging. Nevertheless, MTR and qMT-derived parameters showed a high degree of reproducibility both within the SC and surrounding CSF. CSF-MTR and CSF-PSR coefficients of variation are noted to be relatively elevated, possibly limiting the ability of these measures to detect small differences between patient populations and longitudinal changes within the same subject. Future studies would benefit from CSF-specific MT pulse sequence refinement to reduce these coefficients of variation.

We chose to evaluate the single-point qMT over the “full-fit” model typically used in qMT experiments.²⁷ While the single-point method requires more assumptions than the full model, it can be a useful tool for estimating the PSR in healthy and damaged SC.²⁰ Regarding single-point qMT in the CSF, the assumptions used may not be suitable for extracting true PSR from the CSF, however, to compare with the MTR, we chose to use the single-point model of qMT to

apply corrections to the MTR to remove dependencies on B1, B0, and T1. Further validation of the assumptions for the CSF is necessary to ascertain truer values of the PSR. Incorrect assumptions applied to the single-point model will result in a bias in the observed PSR, however, we feel that the measurements result in consistent indices that are potentially more reproducible than the model-free MTR. A similar argument is made for the calculation of the observed R1, where MFA measurements can bias T1 measurements to a lower value than inversion-recovery-based assessments. Lastly, it is assumed that the exchange rate in CSF is the same as that of spinal cord tissue. We recognize that this assumption needs to be further studied, though previous work has shown that the dependency on the exchange rate for single-point qMT is relatively weak, but can create a bias.

In summary, we understand that the single-point qMT model and the pulse sequence chosen were designed for SC WM and that assumptions as well as model-fitting can result in a bias. However, we show that the calculated indices are reproducible, and correcting for B1, B0, and T1 using the single-point qMT model improves associations, and enhances differences between healthy and MS CSF compared to the standard, uncorrected MTR.

We recruited patients with short disease duration and low clinical disability (EDSS ≤ 2), which may limit the association between WM PSR and EDSS (Figure 4). However, there were statistically significant differences between HC and pwRRMS for PSR in the GM, WM, and CSF (Figure 3). The MTR was not different between HCs and MS patients for GM and WM, but differences within CSF were noted. The lack of MT correlation between WM MT measures with EDSS may relate to the relatively small sample size and small range of EDSS values in this population. However, a continuation of this study would include a larger patient cohort with a wider range of clinical disabilities, age and sex-matched controls, and longitudinal assessment of neurological change as well as changes in tissue abnormality.

A full analysis of CSF samples in congregation with MRI findings would also reveal correlations to biomarkers typically used in the differential diagnosis of MS using CSF. Such tests include measurements of elevated levels of IgG, the presence of MBP, and the CSF/serum albumin ratio, which is an indicator of blood-CSF barrier disruption.²⁸ We also intend to perform lipid and proton magnetic spectroscopy (1H-MRS) on samples from both MS and HC

populations to establish differences in CSF composition and evaluate how these differences are reflected in qMT experiments in vivo.²⁹

This study demonstrated that MT MRI is sensitive to cervical CSF abnormalities in patients with MS and that elevated CSF PSR values correlated with measures of clinical disability. Further comparison of regional CSF MT MRI differences and correlation mass spectrometry laboratory CSF analysis is needed to provide insight into the molecular processes occurring within the CSF in the setting of MS demyelination.

Acknowledgments

The authors would also like to thank the VUIIS technologists (Christopher Thompson, Clair Jones, Leslie McIntosh, and Kristen George-Durett), VUIIS Center for Human Imaging, and Dr Alex Smith for their contributions to this project.

Authors' Notes

Richard D. Lawless and Colin D. McKnight contributed equally to the production of this article.

Declaration of conflicting interests

The authors declared no potential conflicts of interest with respect to the research, authorship, and/or publication of this article.

Funding

The authors would like to acknowledge and thank the sources of funding for this project: Conrad Hilton Foundation (SAS), National MS Society (SAS), NIH/NINDS 1R01NS109114-01 (SAS), NIBIB T32EB021937, and Radiological Society of North America (CDM), NIH/NIBIB 5K01EB030039 (KPO).

ORCID iDs

Richard D. Lawless  <https://orcid.org/0000-0001-8697-3070>
 Colin D. McKnight  <https://orcid.org/0000-0002-4386-8999>
 Kristin P. O'Grady  <https://orcid.org/0000-0002-4550-2026>
 Anna J.E. Combes  <https://orcid.org/0000-0001-8214-5964>
 Atlee A. Witt  <https://orcid.org/0000-0002-2939-263X>

Supplemental material

Supplemental material for this article is available online.

References

1. Wallin MT, Culpepper WJ, Campbell JD, et al. The prevalence of MS in the United States: a population-based estimate using health claims data. *Neurology* 2019; 92: e1029–e1040.
2. Thompson AJ, Banwell BL, Barkhof F, et al. Diagnosis of multiple sclerosis: 2017 revisions of the McDonald criteria. *Lancet Neurol* 2018; 17: 162–173.
3. Barkhof F. The clinico-radiological paradox in multiple sclerosis revisited. *Curr Opin Neurol* 2002; 15: 239–245.
4. Iliff JJ, Wang M, Liao Y, et al. A paravascular pathway facilitates CSF flow through the brain parenchyma and the clearance of interstitial solutes, including amyloid beta. *Sci Transl Med* 2012; 4: 14–7ra11.
5. Ringstad G and Eide PK. Cerebrospinal fluid tracer efflux to parasagittal dura in humans. *Nat Commun* 2020; 11: 354.
6. Kucharczyk W, Macdonald PM, Stanisz GJ, et al. Relaxivity and magnetization transfer of white matter lipids at MR imaging: importance of cerebroside and pH. *Radiology* 1994; 192: 521–529.
7. Schmierer K, Tozer DJ, Scaravilli F, et al. Quantitative magnetization transfer imaging in postmortem multiple sclerosis brain. *J Magn Reson Imaging* 2007; 26: 41–51.
8. Wolff SD and Balaban RS. Magnetization transfer contrast (MTC) and tissue water proton relaxation in vivo. *Magn Reson Med* 1989; 10: 135–144.
9. Koenig SH. Cholesterol of myelin is the determinant of gray-white contrast in MRI of brain. *Magnet Reson Med* 1991; 20: 285–291.
10. Berry I, Barker GJ, Barkhof F, et al. A multicenter measurement of magnetization transfer ratio in normal white matter. *J Magn Reson Imaging* 1999; 9: 441–446.
11. Henkelman RM, Huang X, Xiang QS, et al. Quantitative interpretation of magnetization transfer. *Magn Reson Med* 1993; 29: 759–766.
12. Stanisz GJ, Odobina EE, Pun J, et al. T1, T2 relaxation and magnetization transfer in tissue at 3 T. *Magn Reson Med* 2005; 54: 507–512.
13. Sled JG and Pike GB. Quantitative imaging of magnetization transfer exchange and relaxation properties in vivo using MRI. *Magn Reson Med* 2001; 46: 923–931.
14. Smith AK, By S, Lyttle BD, et al. Evaluating single-point quantitative magnetization transfer in the cervical spinal cord: application to multiple sclerosis. *Neuroimage Clin* 2017; 16: 58–65.
15. Yarnykh VL and Yuan C. Cross-relaxation imaging reveals detailed anatomy of white matter fiber tracts in the human brain. *Neuroimage* 2004; 23: 409–424.
16. Kearney H, Yiannakas MC, Samson RS, et al. Investigation of magnetization transfer ratio-derived pial and subpial abnormalities in the multiple sclerosis spinal cord. *Brain* 2014; 137: 2456–2468.
17. Kurtzke JF. Rating neurologic impairment in multiple sclerosis: an expanded disability status scale (EDSS). *Neurology* 1983; 33: 1444–1452.
18. Held P, Dorenbeck U, Seitz J, et al. MRI of the abnormal cervical spinal cord using 2D spoiled gradient echo multiecho sequence (MEDIC) with magnetization transfer saturation pulse. A T2* weighted feasibility study. *J Neuroradiol* 2003; 30: 83–90.
19. Li K, Dortch RD, Kroop SF, et al. A rapid approach for quantitative magnetization transfer imaging in thigh muscles using the pulsed saturation method. *Magn Reson Imaging* 2015; 33: 709–717.
20. Smith AK, Dortch RD, Dethrage LM, et al. Rapid, high-resolution quantitative magnetization transfer MRI of the human spinal cord. *Neuroimage* 2014; 95: 106–116.

21. Yarnykh VL. Fast macromolecular proton fraction mapping from a single off-resonance magnetization transfer measurement. *Magn Reson Med* 2012; 68: 166–178.
22. Avants BB, Tustison NJ, Song G, et al. A reproducible evaluation of ANTs similarity metric performance in brain image registration. *Neuroimage* 2011; 54: 2033–2044.
23. Fram EK, Herfkens RJ, Johnson GA, et al. Rapid calculation of T1 using variable flip angle gradient refocused imaging. *Magn Reson Imaging* 1987; 5: 201–208.
24. De Leener B, Levy S, Dupont SM, Fonov VS, Stikov N, Louis Collins D, et al. SCT: spinal cord toolbox, an open-source software for processing spinal cord MRI data. *Neuroimage* 2017; 145: 24–43.
25. Chard D and Trip SA. Resolving the clinico-radiological paradox in multiple sclerosis. *F1000Res* 2017; 6: 1828.
26. Bergman J, Svenningsson A, Liv P, et al. Location matters: highly divergent protein levels in samples from different CNS compartments in a clinical trial of rituximab for progressive MS. *Fluids Barriers CNS* 2020; 17: 49.
27. Yarnykh VL. Pulsed Z-spectroscopic imaging of cross-relaxation parameters in tissues for human MRI: theory and clinical applications. *Magn Reson Med* 2002; 47: 929–939.
28. Luque FA and Jaffe SL. Cerebrospinal fluid analysis in multiple sclerosis. *Int Rev Neurobiol* 2007; 79: 341–356.
29. Simone IL, Federico F, Trojano M, et al. High resolution proton MR spectroscopy of cerebrospinal fluid in MS patients. Comparison with biochemical changes in demyelinating plaques. *J Neurol Sci* 1996; 144: 182–190.